LAWRENCE
LIVERMORE
NATIONAL
LABORATORY

LLNL-JRNL-562127

Techniques for correcting velocity and density fluctuations of ion beams

K. M. Woo, S. S. Yu, J. J. Barnard

June 21, 2012

Physical Review Special Topics Accelerators and Beams

Disclaimer

Techniques for correcting velocity and density fluctuations of ion beams

K. M. Woo

Physics Department, The Chinese University of Hong Kong, Hong Kong, China

S. S. Yu

Physics Department, The Chinese University of Hong Kong, Hong Kong, China

Lawrence Berkeley National Laboratory, Berkeley, California 94720, USA

J. J. Barnard

Lawrence Livermore National Laboratory, Livermore, California 94551-0808, USA

Lawrence Berkeley National Laboratory, Berkeley, California 94720, USA

It is well-known that non-uniform voltages in induction accelerator gaps can lead to longitudinal emittance growth, which in turn limits pulse length on target. We show that this source of emittance growth is correctable, even in space charge dominated beams with significant transients induced by space charge waves. Two correction methods are proposed, and their efficacy in reducing longitudinal emittance is demonstrated with three dimensional Particle-In-Cell (PIC) simulations.

I. INTRODUCTION

Longitudinal emittance is a key beam parameter for Heavy Ion Fusion (HIF) since it determines the final bunch length of an ion beam for ignition [Ref. 1]. Beams of short bunch length of 10 nanoseconds or less are required for ignition at target [Ref. 2], the precise bunch length and pulse shape being dependent on details of target designs. For some advanced designs (e.g. for fast ignition), much shorter bunches are required. For many applications in High Energy Density Physics, a short bunch length is also desired. The final length requirements imply that the longitudinal emittance growth must be carefully managed from source to target.

The growth of longitudinal emittance has several complex sources such as the finite temperature and imperfect beam extraction from sources, head-to-tail nonlinearities and other nonlinear space charge effects, as well as voltage non-uniformities in induction linear accelerators. In particular, we will show that longitudinal emittance increases significantly in multi-gap accelerators, in which small fluctuations of individual gap voltages can aggregate over many gaps to give a large value, leading eventually to an unacceptably large growth of longitudinal emittance.

Longitudinal emittance ϵ_z is a quantity that measures beam quality [Ref. 3] and is most directly related to beam pulse length, while the normalized longitudinal emittance ϵ_{zn} is defined by a multiplication of a factor $\beta\gamma$. When there are no other external applied forces, ϵ_{zn} is conserved upon accelerations of beams.

$$\epsilon_z \equiv \frac{4}{\langle v_z \rangle}\sqrt{\langle \Delta z^2 \rangle \langle \Delta v^2 \rangle - \langle \Delta z\, \Delta v \rangle^2}\,. \qquad (1)$$

$$\epsilon_{zn} = \beta\gamma\, \epsilon_z\,. \qquad (2)$$

*Work by one author (JJB) performed under the auspices of the U.S. Department of Energy under contract DE-AC52-07NA27344 at LLNL.

Here $\beta = \frac{\langle v_z \rangle}{c}$ and $\gamma = \frac{1}{\sqrt{1-\beta^2}}$.

γ is taken as 1 since only non-relativistic beams are considered throughout the paper. Also, Δz is the position of particle relative to beam center and Δv_z is the z-component of the particle velocity relative to the overall velocity.

As a beam is extracted from the source, the beam density profile is assumed to be uniform while the velocity profile has a tiny spread due to thermal temperature T at the source which can be approximated by the equipartition theorem. The longitudinal emittance at the source $\epsilon_{zn,s}$ is

$$\epsilon_{zn,s} = \frac{4L}{c\sqrt{12}}\sqrt{\frac{k_B T}{m}}. \qquad (3)$$

Here $\sqrt{\langle \Delta z^2 \rangle} = \frac{L}{\sqrt{12}}$, $\sqrt{\langle \Delta v_z{}^2 \rangle} = \sqrt{\frac{k_B T}{m}}$, and $\langle \Delta z \, \Delta v_z \rangle = 0$ by assuming axisymmetric beam distribution. Also $L = \tau\sqrt{\langle v_z{}^2 \rangle}$, where τ is the pulse duration at source.

Generally, $\epsilon_{zn,s}$ is very small in value as compared to emittance growth resulting from voltage non-unformities. In terms of pulse duration τ, beam energy T and the fractional variation in voltage δ in an injector, ϵ_{zn} [Ref. 1] can be written as

$$\epsilon_{zn} = \frac{4}{m\,c}\tau T \delta. \qquad (4)$$

On the basis of Eq. (4), it has been argued that the pulse length at an HIF injector must be limited. This is of course untrue if this source of emittance growth can be corrected. Effect of multiple non-uniform gap voltages on longitudinal emittance is discussed in this paper and two techniques are presented to reduce the growth of longitudinal emittance by the intermittent application of correction voltages. Our objective is to remove velocity as well as density fluctuations arising from voltage non-uniformities inherent in the accelerating gaps. The correction scheme is particularly non-trivial for space-charge dominated beams, on account of space charge waves which propagate with time. We show by a combination of analyses and simulations with the 3-D PIC code WARP that significant reduction in longitudinal emittance can be achieved.

II. EFFECT OF NON-UNIFORM VOLTAGE ON ϵ_{zn}

Since ϵ_{zn} should be conserved upon acceleration of beams, we show simulation results in three different scenarios to provide self-consistency checks for the code, as well as the basis for comparisons with subsequent calculations.

A. Coasting of an unperturbed beam

A Rubidium beam, 2 MeV, 2.7 microseconds long, and 0.02 mA, passed through a single constant voltage gap and then coasted inside of a pipe. In Fig. 1, a big bump of ϵ_{zn} was observed over the first few microseconds because the beam was in transit through the gap, and a big velocity difference existed between the front and rear parts of the beam. Apart from the bump, ϵ_{zn} remained nearly constant at 3.2×10^{-6} pi-m-rad throughout the coasting, and so ϵ_{zn} due to the thermal temperature at source is conserved.

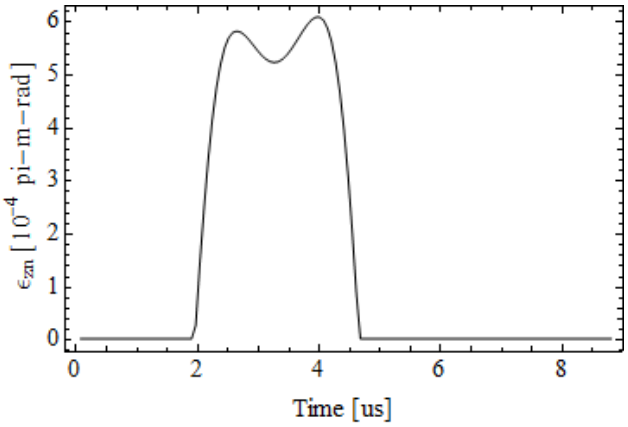

FIG. 1. $\epsilon_{zn}(t)$ evaluated for the whole beam, which was passed through a constant voltage gap.

B. Coasting of a velocity-tilted beam

A Rubidium beam, 2 MeV and of 0.02 mA, with a 10% velocity tilt

$$vtilt \equiv \frac{v_z^{tail} - v_z^{head}}{v_z^{beam}} \times 100\% , \qquad (5)$$

applied at the time of particle loading, coasted inside a pipe. The pulse length changed continually with time. However, according to Liouville's Theorem, ϵ_{zn} must be conserved throughout coasting due to the conservation of phase space area. This conservation property of ϵ_{zn} is verified in Fig. 2, in which ϵ_{zn} is represented by blue circles that fall on the red curve.

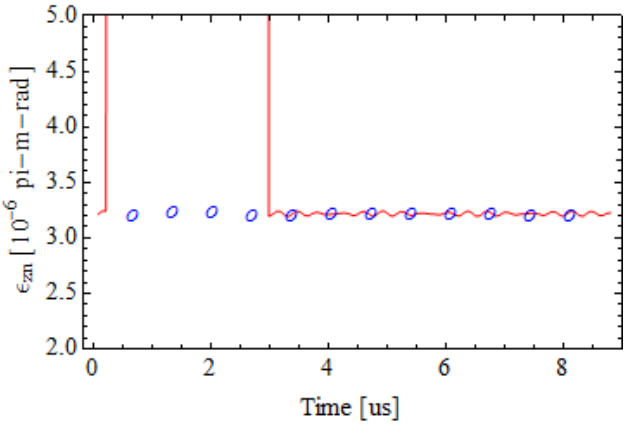

FIG. 2. $\epsilon_{zn}(t)$ evaluated for the whole beam: (1) the curve of blue circles represents a beam coasting with 10% velocity tilt; (2) the red curve represents a beam passing through a constant voltage gap.

C. Effect of many constant voltage gaps

A Rubidium beam, 2 MeV and of 0.02 mA, was passed through many constant voltage gaps. The unnormalized emittance continues to decrease with acceleration, but ϵ_{zn} is unaffected by any changes of beam velocity. In Fig. 3(a), ϵ_{zn} of beams after a constant voltage gap and after 10 constant voltage gaps coincide with the same flat line as 3.2×10^{-6} pi-m-rad verifying that ϵ_{zn} is not affected by acceleration of beams. Meanwhile in Fig. 3(b), ϵ_z was dropped by $\sqrt{2}$ times because the beam velocity was just doubled due to accelerations by 10 gaps .

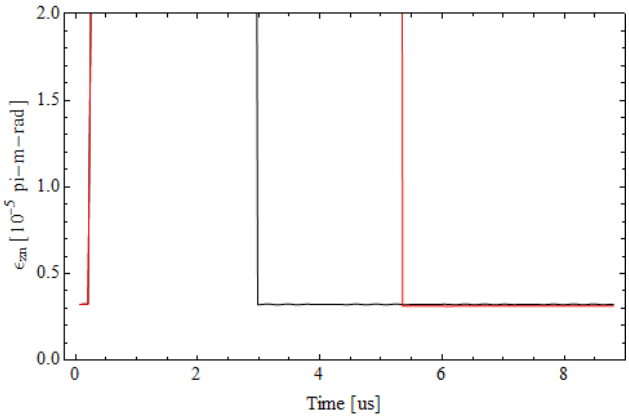

FIG. 3(a). $\epsilon_{zn}(t)$ evaluated for the whole beam: (1) the red curve represents a beam passing through a single constant gap; (2) the black curve represents a beam passing through 10 constant voltage gaps.

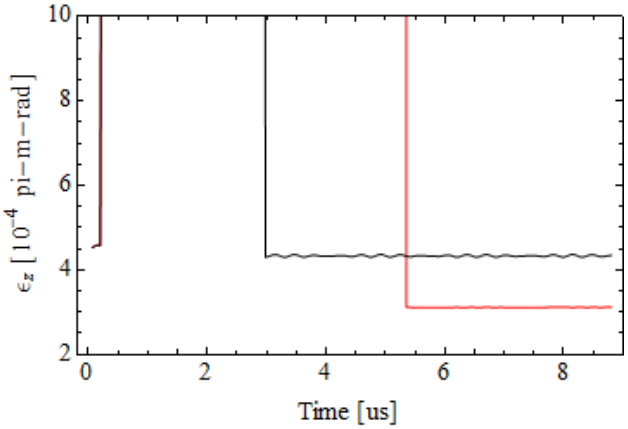

FIG. 3(b). $\epsilon_z(t)$ evaluated for the whole beam: (1) red curve represents a beam passing through a single constant gap; (2) black curve represents a beam passing through 10 constant voltage gaps.

D. Effect of non-uniform voltage gap

We now begin the study of non-uniformity of gap voltage with a gap model of simple sinusoidal variations as errors. Suppose Φ_0 is the desired constant voltage over a gap, $\delta\Phi$ is the amplitude of variation, and $\omega_n \equiv 2n\pi/\tau$ is a particular frequency of the voltage error.

$$\Phi(t) = \Phi_0 + \delta\Phi \sin(\omega_n t)\,. \tag{6}$$

$$v_z(z) = v_{z0} + \delta v_z \sin(k_n z)\,. \tag{7}$$

Here $k_n = \omega_n / v_{z0} = 2n\pi / L$, $z = v_{z0}\, t$, $L = v_{z0}\, \tau$, and $\delta v_z = v_{z0}\, \delta\Phi / 2\Phi_0$. Assume the beam has a uniform line charge density λ_0 such that

$$\left\langle \Delta z^2 \right\rangle = L^2/12$$

$$\left\langle \Delta v_z{}^2 \right\rangle = \delta v_z{}^2/2$$

$$\left\langle \Delta z\, \Delta v_z \right\rangle^2 = \delta v_z{}^2 / k_n{}^2$$

$$\Rightarrow \epsilon_{zn,r} = \frac{4}{c}\sqrt{\frac{L^2}{12}\frac{\delta v_z{}^2}{2} - \frac{\delta v_z{}^2}{k_n{}^2}} = \frac{4L\delta v_z}{c}\sqrt{\frac{1}{24} - \frac{1}{(k_n L)^2}}\,.$$

$$\epsilon_{zn,r} = \frac{2L\delta v_z}{c}\sqrt{\frac{1}{6} - \frac{1}{n^2\pi^2}}\,.$$

Therefore,

$$\epsilon_{zn,r} = 2L\,\delta v_z\; G(n) \tag{8}$$

$$\epsilon_{zn,r} = L\,\delta_\Phi\; v_{z0}\; G(n)\,, \tag{9}$$

here $G(n) = \frac{1}{c}\sqrt{\frac{1}{6} - \frac{1}{n^2\pi^2}}$ and $\delta_\Phi \equiv \frac{\delta\Phi}{\Phi} = 2\frac{\delta v_z}{v_{z0}}$.

In Fig. 4, a Rubidium beam, 2 MeV and of 0.02 mA, was passed through a rippled gap with different errors in two separate simulations. For a 0.2% gap error, the analytic $\epsilon_{zn,r}$ after the gap was 2.23×10^{-5} pi-m-rad, which was about 75% of the simulation value. For a 1% gap error, ϵ_{zn} showed an increase of 5 times that of a 0.2% gap error and it is reasonable since equation (9) shows that the analytic $\epsilon_{zn,r}$ is linearly dependent on the amplitude of variation of voltage.

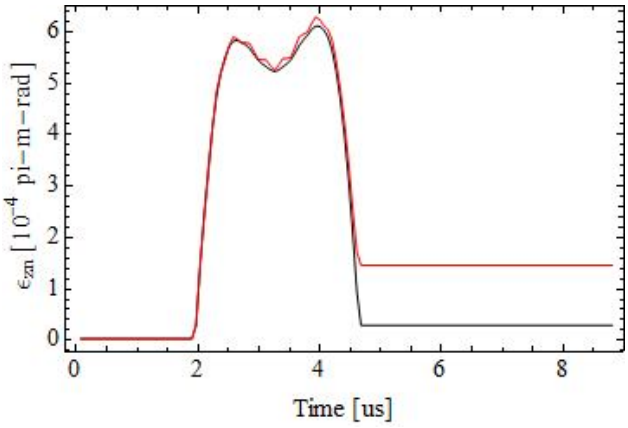

FIG. 4. $\epsilon_{zn}(t)$ evaluated for the whole beam: (1) a gap with 1% error; (2) a gap with 0.2% errors.

In general, the growth of ϵ_{zn} could be huge as the beam continues to pass through many rippled gaps. Because of the random nature of voltage fluctuations, the overall effect on the beam velocity is $\pm\Delta v_z$, ϵ_{zn} will keep on growing in a way similar to random walk. In Fig. 5, ϵ_{zn} was plotted against the number of rippled gaps and ϵ_{zn} was shown increasing with the number of gaps in a square root relation which is similar to a random walk.

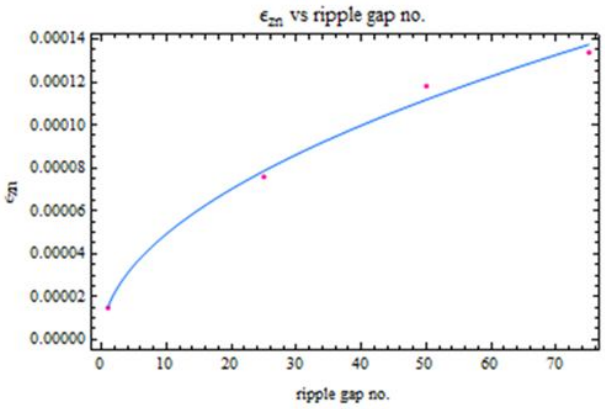

FIG. 5. $\epsilon_{zn}(t)$ evaluated for the whole beam, corresponding to a beam passing through different number of rippled gaps.

III. ONE-STEP CORRECTION

To correct for the growth of longitudinal emittance caused by voltage non-uniformity in gaps, the first idea is simply to measure and to remove velocity ripples directly by imposing an opposite voltage to flatten the velocity profile. This 'one-step correction' was implemented according to the following setup in WARP simulations.

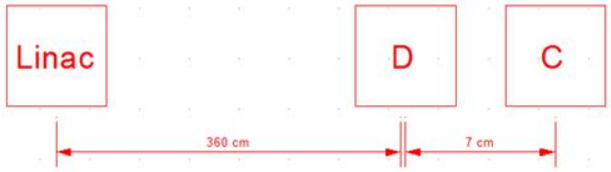

FIG. 6. Setup for one-step correction. Here D is the position of the velocity diagnostic and C is the position of the velocity correction.

For the purpose of this paper, we assume that a precise diagnostic for the energy profile exists. (We will show in a separate paper that a non-invasive energy diagnostic is in fact possible at any nonrelativistic energy.) The beam kinetic energy is measured at position D, and the corresponding beam velocity profile at position C is calculated via the static time of flight according to velocity data from D to C. To remove all velocity ripples, an opposite velocity waveform is generated at position C by applying the corresponding correction voltage. In this scheme, the density ripples at D remain uncorrected.

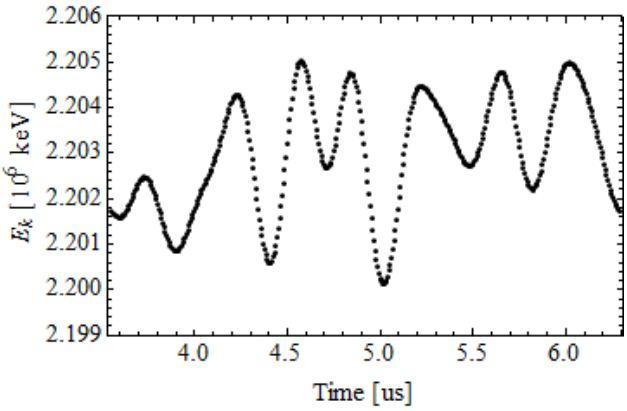

FIG. 7. Kinetic energy of the beam at position D.

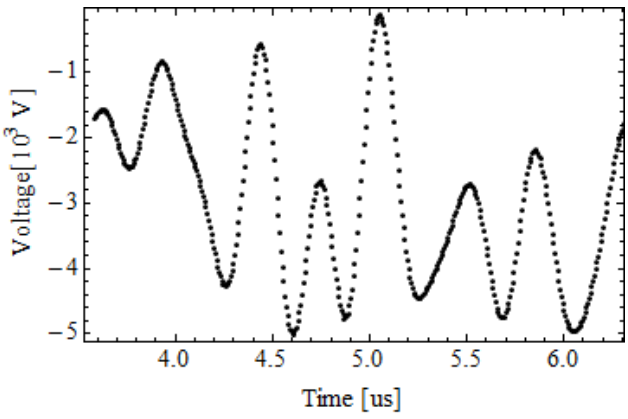

FIG. 8. Correction voltage applied at position C.

As an example, Fig. 7 was the kinetic energy profile detected at D, while Fig. 8 was the correction voltage applied at position C to remove the velocity ripples. Consequently, a significant reduction of ϵ_{zn} was observed in Fig. 9 after the one-step correction from 12.79×10^{-5} pi-m-rad to 3.226×10^{-6} pi-m-rad, a value which is very close to the original value before the emittance growth.

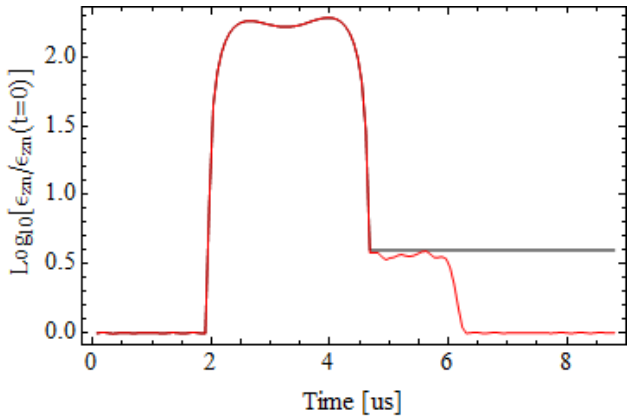

FIG. 9. Reduction of $\in_{zn}$ after the application of correction voltage: (1) black curve represents a beam without correction voltage applied; (2) red curve represents a beam with correction voltage applied.

A. Criteria for one-step correction

The question we would next address is how often the correction has to be performed in a multi-gap LINAC. Particle over-taking is the main concern determining the success of one-step correction for low current beams, in which space-charge waves are weak. The critical downstream distance before particle over-taking based on a sinusoidal pulse is derived here.

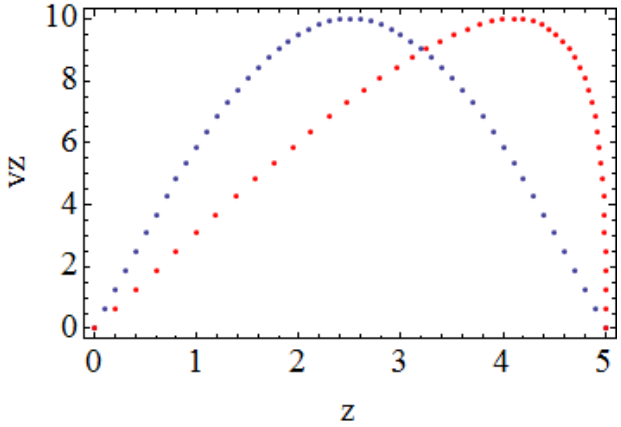

FIG. 10. Diagram of particle over-taking in $v_z - z$ phase space.

Suppose a beam has a uniform longitudinal particle distribution and a velocity perturbation in sinusoidal waveform with width L, which is represented by blue dots in Fig. 10. Within the velocity pulse, N particles are uniformly located and they are labeled by index n.

$$z_n = \frac{L}{N} n \quad \text{and} \quad L = \frac{\lambda}{2}. \tag{10}$$

$$v_1 = \delta v \sin(k z_n) \quad \text{and} \quad k = \frac{2\pi}{\lambda}. \tag{11}$$

After some time $\Delta t = \frac{\Delta z}{v_{z0}}$, each particle move to

$$\tilde{z}_n = z_n + v_1(z_n)\Delta t, \tag{13}$$

Over-taking appears when $\left(\frac{d\tilde{z}}{dn}\right)_{n=N} = 0$,

in terms of wavelength λ_m, and frequency f_m,

$$\lambda_m = \frac{\lambda_0}{m} = \frac{\tau_0 v_{z0}}{m} = \frac{v_{z0}}{f_m} \quad \text{and let} \quad P \equiv \frac{\delta v_z}{2 v_{z0}}.$$

Therefore, the critical downstream distance is

$$\Delta z \approx \frac{v_{z0}}{\pi f_m P}. \tag{14}$$

For example, a Rubidium beam, 2 MeV and 0.02 mA, was passed through a series of gaps at interval of 0.72 m; each gap provides energy 0.1×2 MeV for accelerations but each gap voltage also has sinusoidal perturbations with magnitude 0.001×2 MeV and were composed of different modes (m = 1, 2, …, 10), i.e. corresponding ripple frequencies vary from 0.37 to 3.7 MHz. In these examples, particle over taking appeared after 70 gaps meaning that this is the longest interval to install the next one-step correction.

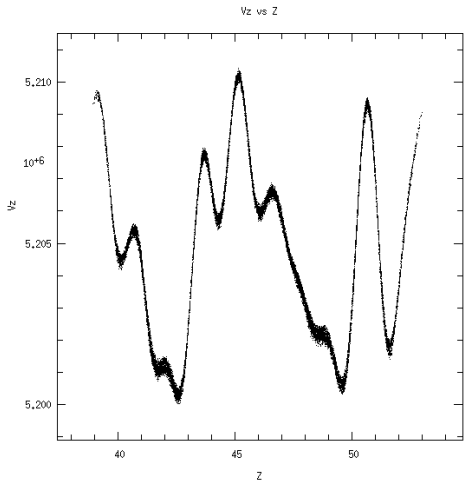

FIG. 11(a). *vz-z* phase space after 50 gaps.

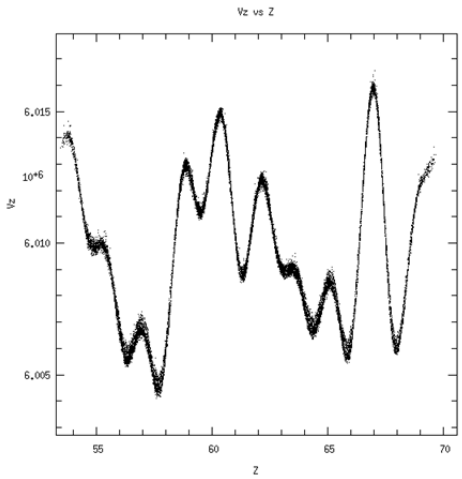

FIG. 11(b). *vz-z* phase space after 70 gaps.

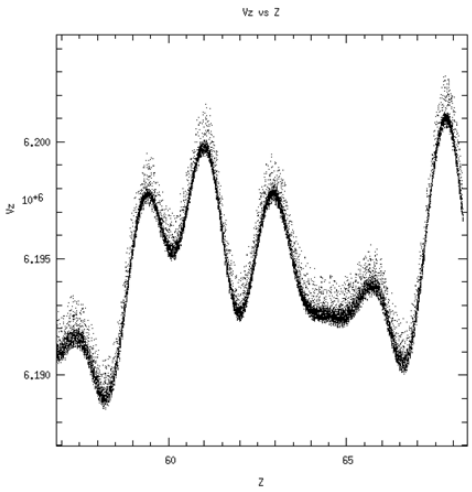

FIG. 12. *vz-z* phase space after 75 gaps.

B. Space-charge dominated beam at high current

Actually, one-step correction would be less effective in space-charge dominated beams at high current due to evolution of space-charge waves, leading to substantial growing ripples in both density and velocity profiles. One-step correction assuming static time of flights of velocity profile over 7 cm in course of simulations could be inaccurate if velocity ripples evolve. This evolution actually happens to a high current beam. In addition, growing density ripples were not removed in this correction method. Fig. 13 compares the difference of ϵ_{zn} after one-step correction for low current beam — 0.02 mA (blue curve) and the high current beam — 0.02 A (red curve). Clearly, longitudinal emittance is not well suppressed by one-step correction for a high current beam so ϵ_{zn} was found to increase very soon after correction.

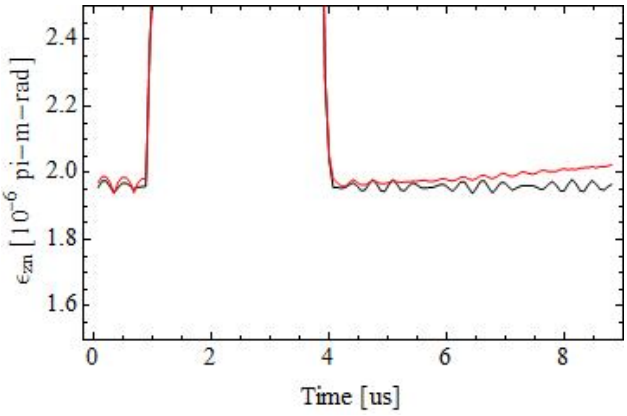

FIG. 13. Comparison of one-step corrections between low and high current beams: (1) black curve represents the low current beam, 0.02 mA; (2) red curve represents the high current beam, 0.02 A.

Besides the evolution of space charge waves, head-to-tail nonlinear space-charge effects also account for a significant growth of longitudinal emittance. (See the comparison in Fig. 14.) The big velocity difference between the head and the tail of a beam due to space-charge can be quite big. The effect of head-to-tail non-linearity [Ref. 4] is not the focus of this paper, and

can be avoided by adding 'ear fields' to keep the head and tail at constant energy over time. Unless specified, all following simulations will have ear fields.

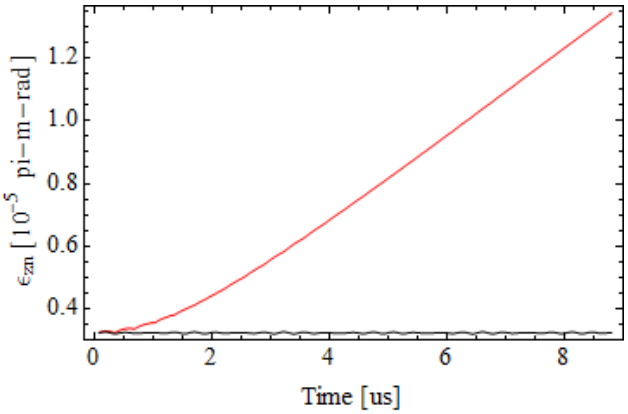

FIG. 14. $\epsilon_{zn}(t)$ evaluated for the whole beam: (1) red curve represents high current 0.2 A; (2) black curve represents low current 0.2 mA.

IV. TWO-STEP CORRECTION

A. General evolution of space-charge waves

To trace the dynamics of velocity and density waves, the general evolution of space-charge waves was derived here based on weak perturbations of 1-D fluid model [Ref. 5, 6 and 7]. Obtained wave solutions for velocity and density waves were used to compute the required correction voltages that help to remove all ripples in both velocity and density profiles. The general idea of two-step correction is discussed in the following section B and the terms of "ripples" and "waves" are used interchangeably in the following text.

Consider continuity and momentum equations the in z-direction

$$\frac{\partial \lambda}{\partial t}+\frac{\partial(\lambda v_z)}{\partial z}=0\,, \tag{15a}$$

$$\frac{\partial v_z}{\partial t}+v_z\frac{\partial v_z}{\partial z}=\frac{q}{m}E_z\,. \tag{15b}$$

λ is the line charge density, q is the ion charge, m is the ion mass and E_z is the longitudinal self-electric field, which is approximated by

$$E_z \approx -g\frac{\partial \lambda}{\partial z}\,, \tag{16}$$

where $g=\dfrac{1}{2\pi\varepsilon_0}\ln(b/a)$.

b/a is the ratio of the pipe radius to the mean beam radius and g is the g-factor. By substituting $v_z = v_{z0}+v_1$, $\lambda=\lambda_0+\lambda_1$, and taking the first order approximation, thus the wave equation for the density ripple is obtained, where the space-charge wave speed is denoted by c_s. The solution of velocity wave v_1 can be obtained by considering equation (15a) after solving for λ_1.

$$\frac{\partial^2 \lambda_1}{\partial t'^2}-c_s{}^2\frac{\partial^2 \lambda_1}{\partial z'^2}=0\,, \tag{17}$$

where $c_s=\sqrt{\dfrac{q\,g\,\lambda_0}{m}}$.

The Subscript 0 represents equilibrium value while the subscript 1 represents the perturbed part of that quantity. t' and z' are measured in beam frames but lab frames are used in following text. The general wave solution is a pair of a forward-moving wave ξ_+ and a backward-moving wave ξ_- and they are solved by acquiring well-posed boundary conditions. General wave solutions are

$$\begin{cases}\lambda_1(t,z)=\lambda_0\left[\xi_+\left(t-\dfrac{z}{v_{z0}+c_s}\right)+\xi_-\left(t-\dfrac{z}{v_{z0}-c_s}\right)\right]\\ v_1(t,z)=c_s\left[\xi_+\left(t-\dfrac{z}{v_{z0}+c_s}\right)-\xi_-\left(t-\dfrac{z}{v_{z0}-c_s}\right)\right]\end{cases}. \tag{18}$$

Denote voltages by $\Phi=\Phi_0+\Phi_1$,

and define $f_i\equiv\left(\dfrac{\Phi_1}{\Phi_0}\right)_{at\ z_i}$.

At $z=0$, let the boundary conditions to be

$$\begin{cases} v_1(t, z=0) = v_1(t) \\ \lambda_1(t, z=0) = \lambda(t) \end{cases}. \tag{19}$$

On solving ξ_+ and ξ_- gives

$$\begin{cases} \xi_+(t) = \frac{1}{2}\left[\frac{v_1(t)}{c_s} + \frac{\lambda_1(t)}{\lambda_0}\right] \\ \xi_-(t) = \frac{1}{2}\left[-\frac{v_1(t)}{c_s} + \frac{\lambda_1(t)}{\lambda_0}\right] \end{cases} \tag{20}$$

Define phase factors $\varphi_\pm(z) = \dfrac{z}{v_{z0} \pm c_s}$

Therefore, general waves propagation are

$$\begin{cases} v_1(t,z) = \frac{1}{2}\left[v_1(t-\varphi_+) + v_1(t-\varphi_-)\right] + \frac{c_s}{2\lambda_0}\left[\lambda_1(t-\varphi_+) - \lambda_1(t-\varphi_-)\right] \\ \lambda_1(t,z) = \frac{\lambda_0}{2\,c_s}\left[v_1(t-\varphi_+) - v_1(t-\varphi_-)\right] + \frac{1}{2}\left[\lambda_1(t-\varphi_+) + \lambda_1(t-\varphi_-)\right] \end{cases}$$

B. Principle of two-step correction

Knowing the complete solutions of λ_1 and v_1 is particularly important since they allow us to predict their waveform at any time and position. With this knowledge, we can apply "correction voltages" to generate "opposite waveforms" that lead to zero fluctuations in their profiles. This technique is called the two-step correction because two correction voltages are applied separately at two different positions.

Our simulation exercise was generated as follows: a beam was first loaded without any disturbance in both density and velocity profiles; then it was passed through the first gap $f_0(t)$, which serves as the source of voltage fluctuations. The first step is done by applying a specified voltage $f_1(t)$ at z_1 to generate an another density wave that exactly cancel the one generated by $f_0(t)$ at z_2. Consequently, the overall density wave is now made to be zero right at z_2. At the same time, the second step is done by applying of a specified voltage $f_2(t)$ at z_2 to generate an another velocity wave that exactly cancel the one generated by $f_0(t)$ and $f_1(t)$ at z_2. Therefore, zero fluctuations for both λ_1 and v_1 is achieved for all time after position z_2, resulting in an effective reduction of ε_{zn} for space-charge dominated beams.

FIG. 15. Setup for two-step correction.

C. Solving voltage $f_0(t)$ for density ripples correction

Knowing the waveform of correction voltages is the key part of this two-step correction technique.

At z_0 the boundaries take the following form

$$\begin{cases} \lambda_1(t) = 0 \\ v_1(t) = \dfrac{v_{z0}}{2}\left(\dfrac{\Phi_1(t)}{\Phi_0}\right)_{at\ z_0} = \dfrac{v_{z0}}{2} f_0(t) \end{cases}. \tag{21}$$

When $f_1(t)$ is absent and the density wave at z_2 is

$$\lambda_1(t,z) = \frac{\lambda_0 v_{z0}}{4c_s}\left[f_0\left(t - \frac{z}{v_{z0}+c_s}\right) - f_0\left(t - \frac{z}{v_{z0}-c_s}\right)\right]. \tag{22}$$

When f_1 is present and the density wave at z_2 becomes

$$\lambda_1(t,z) = \frac{\lambda_0 v_{z0}}{4c_s}\left[f_0\left(t - \frac{z_2}{v_{z0}+c_s}\right) - f_0\left(t - \frac{z_2}{v_{z0}-c_s}\right) + f_1\left(t - \frac{z_2 - z_1}{v_{z0}+c_s}\right) - f_1\left(t - \frac{z_2 - z_1}{v_{z0}-c_s}\right)\right]. \tag{23}$$

Denote $F_0(t) \equiv f_0\left(t - \dfrac{z_2}{v_{z0}+c_s}\right) - f_0\left(t - \dfrac{z_2}{v_{z0}-c_s}\right)$,

and $F_1(t) \equiv f_1\left(t - \dfrac{z_2 - z_1}{v_{z0}+c_s}\right) - f_1\left(t - \dfrac{z_2 - z_1}{v_{z0}-c_s}\right)$.

Notice that the application of voltage $f_1(t)$ leads to generation of an another density wave $F_1(t)$, but this voltage $f_1(t)$ is specially designed in a way that zero density fluctuation at z_2 results i.e.:

$$\begin{cases} \lambda_1(t, z_2) = 0 \\ F_0(t, z_2) + F_1(t, z_2 - z_1) = 0 \end{cases}. \quad (24)$$

Therefore, the above condition constrains the allowed form of $f_1(t)$ at z_1. To solve for $f_1(t)$, expand $f_1(t)$ into a Fourier series

$$f_1(t) = \sum_{n=-\infty}^{+\infty} c_n \, e^{i\omega_n t}, \quad (25)$$

here $\omega_n = \dfrac{2n\pi}{T}$ and T is the pulse life.

On solving the lower of Eq. (24), the required c_n can be found:

$$c_n = \frac{\dfrac{1}{T}\displaystyle\int_{t_1}^{t_2} -F_0(t, z_2)\, e^{-i\,\omega_n\, t}\, dt}{e^{-i\omega_n\left(\frac{z_2 - z_1}{v_{z0} + c_s}\right)} - e^{-i\omega_n\left(\frac{z_2 - z_1}{v_{z0} - c_s}\right)}}. \quad (26)$$

D. Solving voltage f_2 for velocity ripples correction

Since $f_1(t)$ is now known and the overall velocity waves generated by $f_0(t)$ and $f_1(t)$ are given by:

$$v_1(t, z) = \frac{v_{z0}}{4}\left[f_0\left(t - \frac{z_2}{v_{z0} + c_s}\right) + f_0\left(t - \frac{z_2}{v_{z0} - c_s}\right) + f_1\left(t - \frac{z_2 - z_1}{v_{z0} + c_s}\right) + f_1\left(t - \frac{z_2 - z_1}{v_{z0} - c_s}\right)\right]. \quad (27)$$

Therefore, the velocity wave $v_1(t, z_2)$ can be removed by applying the corresponding opposite voltage f_2 in the same way as in one-step correction,

$$f_2(t) = -\frac{v_1(t, z_2)}{v_{z0}} \times 2. \quad (28)$$

E. Simulation parameters

The two-step correction scheme can be investigated via WARP simulations of a Rb beam with the following beam parameters.

Table I Summary of beam parameters [Ref. 8, 9, 10, 11]

Ion species: Rubidium (charged +1)
Current: 20 mA
KE: 2 MeV
Un-normalized transverse emittance: 52 mm m-rad
Mean beam radius: 0.016 m

In simulations, the source of voltage fluctuations $f_0(t)$ is modeled by

$$f_0(t) = \mathbb{N}\sum_{n=1}^{10} \sin\left(\frac{2n\pi}{T}t + \alpha_n\right) + \cos\left(\frac{2n\pi}{T}t + \beta_n\right). \quad (29)$$

Here $\mathbb{N}$ is a normalization factor to make the value of root-mean-square of $f_0(t)$ close to 0.1% of the beam energy. We further assume the waveform of $f_0(t)$ is known and detectable. Because of the special purpose of the voltage $f_1(t)$ to achieve zero density fluctuation at z_2, we call this voltage as the Density Error Correction voltage (DEC). Similarly, because of the purpose of voltage $f_2(t)$ to achieve zero velocity fluctuation at z_2, we call this voltage the Velocity Error Correction (VEC).

1. Result of DEC at z_2

Fig. 16 showed a line charge density profile $\lambda(t)$ at z_2 : (1) The blue curve represented the $\lambda(t)$ of a beam without any corrections, in which density ripples were found. (2) The red curve represented the $\lambda(t)$ of a beam with the application of the DEC voltage at z_1 but

density ripples were removed effectively by the application of $f_1(t)$.

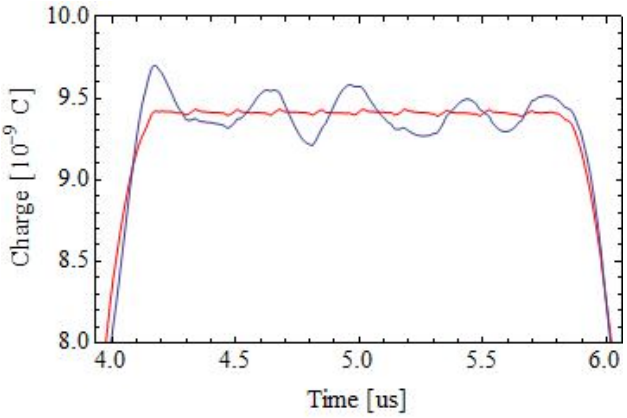

FIG. 16. Result of DEC at z_2 . (See text for explanation of red and blue curves)

2. Result of VEC at $z_2 + 0.72m$

Fig. 17 shows the profile of the velocity $v_z(t)$ at $z_2 + 0.72m$: (1) The blue curve represented a beam after DEC at z_1 and velocity ripples were found. (2) The red curve represented a beam after DEC at z_1 and VEC at z_2 but velocity ripples were removed effectively removed.

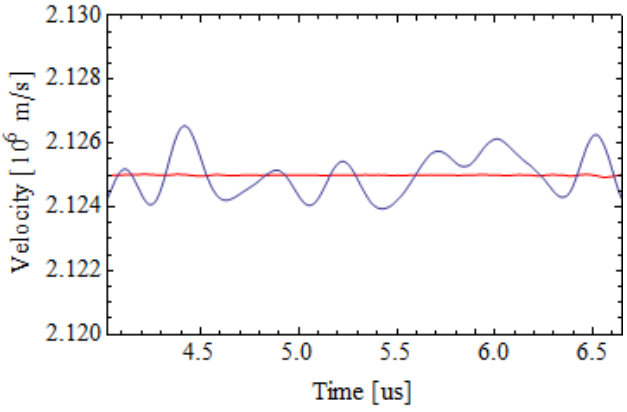

FIG. 17. Result of VEC at $z_2 + 0.72m$

3. Result of reduction of ε_{zn}

Based on Fig. 16 and Fig. 17, we can see clearly how density ripples and velocity ripples were removed by two-step corrections, as a result, the growth of longitudinal emittance is suppressed. Fig. 18 is the $\in_{zn}$ of three beams: (1) The blue curve represented the $\in_{zn}$ of a beam after one-step correction. (2) The red curve represented the $\in_{zn}$ of a beam after two-step correction. (3) The black curve represented a beam without any corrections. Clearly, the beam without corrections showed a huge increase of $\in_{zn}$ after passing through the first gap $f_0(t)$. Although both one-step and two-step corrections lead to similar amount of reduction in $\in_{zn}$, a big advantage of two-step correction is that the $\in_{zn}$ will not grow again after z_2 for all time and this was understood because the density fluctuation is suppressed by $f_1(t)$.

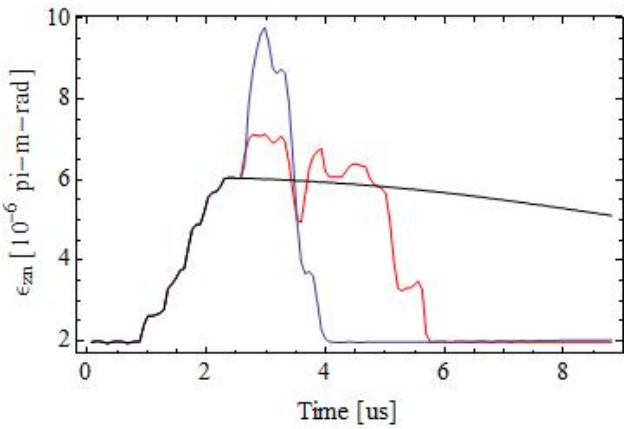

FIG. 18(a). one-step v.s. two-step corrections.

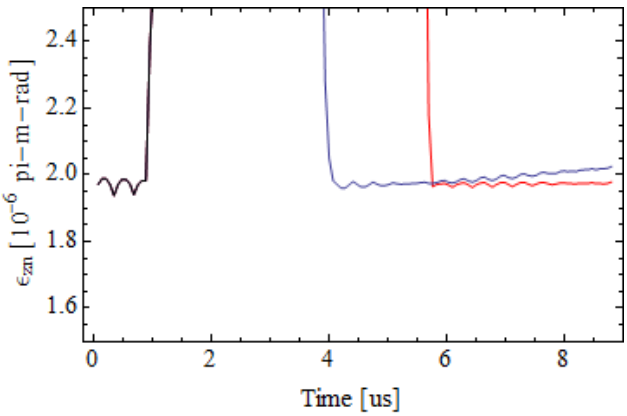

FIG. 18(b). A bigger view of Fig. 18(a).

V. Conclusion

We show that whenever energy and current profiles are measured after a series of gaps by non-invasive means, space-charge waves are traced completely and perturbations in velocity and density profiles can be removed by applications of designated voltages. Therefore, both techniques of one-step and two-step corrections succeed to reduce $\in_{zn}$ significantly even in space-charge dominated beams, implying that the fundamental limit on pulse length at source can be relaxed in near term as well as driver-scale experiments of Heavy Ion Fusion. In addition, these correction techniques can be extended for high energy density physics and other intense beam applications whenever non-uniform voltages appear.

References

1. P. A. Seidl, E. P. Lee, R. O. Bangerter and A. Faltens, "An Induction Linac Driver For A 0.44 MJ Heavy-Ion Direct Drive Target", Lawrence Berkeley National Laboratory, University of California, Berkeley, California, USA, February 8, 2010

2. S. S. Yu, "An Updated Point Design For Heavy Fusion", Lawrence Berkeley National Laboratory, University of California, Berkeley, California, USA

3. M. Reiser, "Theory and Design of Charged Particle Beams"

4. Lau Yuk Yeung, "Final Compression Beamline Systems for Heavy Ion Fusion Drivers", Thesis for Master of Philosophy in Physics, The Chinese University of Hong Kong, Hong Kong, China

5. John Barnard, HIF note 96-12, Subject: "Implications of Pulser Voltage Ripple", September 24, 1996, Lawrence Livermore National Laboratory

6. J. G. Wang, D. X. Wang, D. Kehne, and M. Reiser, "Generation of Space-Charge Waves due to Localized Perturbations", Laboratory for Plasma Research and Department of Electrical Engineering, University of Maryland, College Park

7. K. Tian,* R. A. Kishek, I. Haber, M. Reiser, and P. G. O'Shea, "Experimental study of large-amplitude perturbations in space-charge dominated beams", Institute for Research in Electronics and Applied Physics, University of Maryland, College Park, Maryland, USA, published 8 March 2010

8. E. P. Lee and R. K. Cooper, "General Envelope Equation For Cylindrically Symmetric Charged-Particle Beams", Particle Accelerators, 1976, Vol. 7, 83-95

9. O. A. Anderson, "Accurate iterative analytic solution of the Kapchinskil-Vladimirskij equations for the cases of a matched beam", Lawrence Berkeley National Laboratory, University of California, Berkeley, California, USA, October 1, 2006

10. Stanley Humphries, Jr., "Principles of Charged Particle Acceleration", Department of Electrical and Computer Engineering, University of New Mexico, Albuquerque, New Mexico

11. Stanley Humphries, Jr., "Charged Particle Beams", Department of Electrical and Computer Engineering, University of New Mexico, Albuquerque, New Mexico